RMetS Royal Meteorological Society

# The morphology of the Brewer–Dobson circulation and its response to climate change in CMIP5 simulations

Steven C. Hardiman[a]* Neal Butchart[a] and Natalia Calvo[b]
[a] Met Office Hadley Centre, Exeter, UK
[b] Dpto Física de la Tierra II, Universidad Complutense de Madrid, Spain

*Correspondence to: S. C. Hardiman, Met Office Hadley Centre, FitzRoy Road, Exeter, Devon EX1 3PB, UK.
E-mail: steven.hardiman@metoffice.gov.uk



**This article analyses the annual mean vertical and latitudinal structure of the Brewer–Dobson circulation in the CMIP5 models. The strength of the tropical mass upwelling is found to increase at all altitudes throughout the stratosphere due to climate change. However, the width of the tropical upwelling region narrows below about 20 hPa, and widens above 20 hPa, suggesting different physical mechanisms may play a role in this change above and below 20 hPa. In the lower stratosphere, an equatorward shift in the stationary wave critical line allows waves to propagate further into the Tropics. However, in the upper stratosphere, where the behaviour is dominated by what happens during the winter, an increase in the extratropical zonal mean westerly jet leads to a reduced equatorward refraction of planetary waves. The seasonal cycle of the change in the Brewer–Dobson circulation is also considered, and differences are found in the latitudinal structure of the increased extratropical downwelling between the Northern and Southern Hemispheres in winter.**

*Key Words:* Brewer–Dobson circulation; stratosphere; CMIP5

*Received 19 December 2012; Revised 22 August 2013; Accepted 16 September 2013; Published online in Wiley Online Library*

## 1. Introduction

The Brewer–Dobson circulation describes the Equator-to-pole stratospheric meridional mass circulation. It plays an important role in determining the thermal structure of the stratosphere and also in transporting chemical species into, within and out of the stratosphere. The strength of the Brewer–Dobson circulation has generally been defined by the tropical upwelling mass flux through 70 hPa (Butchart and Scaife, 2001; Butchart *et al.*, 2006, 2010; McLandress and Shepherd, 2009). This altitude is sufficiently high to be above two-way stratosphere–troposphere exchange, and sufficiently low to avoid the complications of in-mixing from the Extratropics (Neu and Plumb 1999). The Tropics also exhibit upwelling at all latitudes, unlike the Extratropics where anomalous secondary circulations can complicate interpretations of the strength of the meridional circulation.

The tropical upwelling through 70 hPa remains a good single-number measure for the strength of the Brewer–Dobson circulation. Using this definition, previous modelling studies (Butchart *et al.*, 2006, 2010) have established the result that the strength of the Brewer–Dobson circulation is predicted to increase in almost all models under climate change. However, Boenisch *et al.* (2011) have shown that changes in tropical upwelling in the lowermost stratosphere do not necessarily describe changes in the Brewer–Dobson circulation throughout the stratosphere. In particular, they distinguish two separate branches of the circulation, a 'shallow branch' in the subtropical lower stratosphere and a 'deep branch' reaching the upper stratosphere (Plumb, 2002; Birner and Boenisch, 2011). Thus, whilst at any given pressure level the change in tropical upwelling must be balanced by a change in extratropical downwelling, changes in the spatial structure of the downwelling would not be so described. Furthermore, the width of the upwelling region is likely to alter due to climate change (McLandress and Shepherd, 2009; Li *et al.*, 2010). These articles clearly indicate the need for a more detailed study of the spatial structure of the Brewer–Dobson circulation. In particular, the extratropical downwelling component of the Brewer–Dobson circulation has not been considered in detail by previous multi-model studies, though McLandress and Shepherd (2009) considered this in Canadian Middle Atmosphere Model (CMAM) simulations.

The Coupled Model Intercomparison Project 5 (CMIP5; http://cmip-pcmdi.llnl.gov/cmip5) model simulations provide a good resource for such a multi-model study. Until now, the Brewer–Dobson circulation and its response to climate change has largely been investigated in models that have a well-resolved stratosphere but are not coupled to an ocean model. The CMIP5 simulations provide, for the first time, a multi-model ensemble of coupled atmosphere–ocean models with

Table 1. CMIP5 models included in this study.

| Model | Institute | Number of levels | Lid height | Scenario |
|---|---|---|---|---|
| CESM1-WACCM | NSF-DOE-NCAR | 66 | $5.96\times10^{-6}$ hPa | Historical, RCP 8.5 |
| CMCC-CESM | CMCC | 39 | 0.01 hPa | RCP 8.5 |
| CMCC-CMS | CMCC | 95 | 0.01 hPa | Historical |
| EC-EARTH | EC-EARTH | 91 | 0.01 hPa | Historical |
| GFDL-CM3 | NOAA GFDL | 48 | 0.01 hPa | Historical |
| GISS-E2-R | NASA GISS | 40 | 0.1 hPa | Historical, RCP 8.5 |
| HadGEM2-CC | MOHC | 60 | 85 km | Historical, RCP 8.5 |
| IPSL-CM5A-LR | IPSL | 39 | 0.04 hPa | Historical, RCP 8.5 |
| MIROC-ESM | MIROC | 80 | 0.0036 hPa | Historical, RCP 8.5 |
| MIROC-ESM-CHEM | MIROC | 80 | 0.0036 hPa | Historical, RCP 8.5 |
| MPI-ESM-LR | MPI-M | 47 | 0.01 hPa | Historical, RCP 8.5 |
| MRI-CGCM3 | MRI | 48 | 0.01 hPa | Historical |

Acronyms:
CESM Community Earth System Model; CMCC Centro Euro-Mediterraneo sui Cambiamenti Climatici (Italy);
DOE Department of Energy (USA); EC European Community; GFDL Geophysical Fluid Dynamics Laboratory (USA);
GISS Goddard Institute for Space Studies (USA); HadGEM Hadley Centre Global Environment Model;
IPSL Institut Pierre-Simon Laplace (France); MIROC Model for Interdisciplinary Research on Climate (Japan);
MOHC Met Office Hadley Centre (UK); MPI Max Planck Institute (Germany);
MRI Meteorological Research Institute (Japan); NSF National Science Foundation (USA);
NASA National Aeronautics and Space Administration (USA); NCAR National Center for Atmospheric Research (USA);
NOAA National Oceanic and Atmospheric Administration (USA); WACCM Whole Atmosphere Community Climate Model.

a well-resolved stratosphere and well-represented stratospheric processes (Charlton *et al.*, 2013).

In this study, the climate change response in the structure of tropical upwelling and the width of the tropical upwelling region in the models is analysed. In particular, the role of changes in planetary wave propagation is investigated. The seasonal cycle of the tropical upwelling region is also analysed, specifically to gain a view on how the change in tropical upwelling is balanced by changes in extratropical downwelling.

## 2. CMIP5 models and simulations

The CMIP5 model simulations used in this study are as follows:

- Historical simulations run from 1860 to 2005. These are forced by observed concentrations of long-lived greenhouse gases and reconstructed aerosol emissions, and also include solar and volcanic forcings. The period 1960–2000 is analysed in this article.
- Climate change projections start from the end of the historical simulation, and run from 2006 to 2100. The future scenario used here is Representative Concentration Pathway (RCP) 8.5 (Riahi *et al.*, 2007; Moss *et al.*, 2010), corresponding to a rise in radiative forcing to a value of about 8.5 W m$^{-2}$ by 2100. In the HadGEM2-ES model, this leads to an increase in globally averaged near-surface temperatures of almost 6 K by 2100 compared to pre-industrial values (Caesar *et al.*, 2013).

The Brewer–Dobson circulation is generally diagnosed using the residual vertical velocity (defined in the next section). However, this variable was not available in the central CMIP5 archive. Thus data had to be obtained directly from the modelling groups, and was available from only a subset of models (Table 1; eleven and eight models for the historical and RCP 8.5 simulations, respectively). Since daily dynamical fields were not available on sufficient vertical levels, only monthly mean data are used throughout this study. All models used are stratosphere resolving or 'high-top' models, with upper boundary above 1 hPa (e.g. Charlton *et al.*, 2013). The Brewer–Dobson circulation analysed in a limited number of models with upper boundaries below 1 hPa was found to be too weak compared to reanalysis data. Only one ensemble member is used for each model. Further details can be found in Charlton *et al.* (2013) and individual model documentation papers (Lott *et al.*, 2005; Hazeleger *et al.*, 2010; Jones *et al.*, 2011; Marsh *et al.*, 2013).

## 3. Annual mean

### 3.1. The residual mean circulation

In this article, the transformed Eulerian mean residual circulation, $(\overline{v}^*, \overline{w}^*)$, is used to diagnose the Brewer–Dobson circulation. This can be considered the wave-driven part of the stratospheric meridional circulation (Andrews *et al.*, 1987), p. 128 where

$$\overline{v}^* \equiv \overline{v} - \frac{1}{\rho_0}\left(\frac{\rho_0 \overline{v'\theta'}}{\overline{\theta}_z}\right)_z, \tag{1}$$

$$\overline{w}^* \equiv \overline{w} + \frac{1}{a\cos\phi}\left(\frac{\cos\phi\,\overline{v'\theta'}}{\overline{\theta}_z}\right)_\phi. \tag{2}$$

Here overbars indicate a zonal mean, and primes indicate a deviation from the zonal mean, $v$ is the meridional velocity, $w$ is vertical velocity, $\rho_0$ is density, $a$ is the Earth's radius, $z$ is log-pressure height, and $\theta$ is potential temperature.

Figure 1 shows the annual mean climatological $\overline{w}^*$ derived from ERA-Interim (1989–2009; Dee *et al.*, 2011; Seviour *et al.*, 2012), and the CMIP5 multi-model mean (1960–2000). The distribution with height in ERA-Interim shows two local maxima, one in the lowermost stratosphere (100 hPa) and one above about 5 hPa. This feature is also captured in the models. There is a local minimum in $\overline{w}^*$ at the Equator and a peak in the Subtropics, centred at about 60 hPa, shown also in both ERA-Interim and the multi-model mean.

The region where $\overline{w}^* > 0$, extending from approximately 35°S to 35°N for the annual mean, will be referred to as the 'tropical upwelling region'. The edges of this region, where $\overline{w}^* = 0$, are called the 'turn-around latitudes' (Rosenlof, 1995).

Also shown in Figure 1 is the stream function (grey contour lines)

$$\psi = \int \rho_0 a\cos(\phi)\overline{w}^*\,\mathrm{d}\phi. \tag{3}$$

The residual circulation is along lines of constant $\psi$, and $\psi$ has the property of being a maximum/minimum at the northern/southern turn-around latitudes.

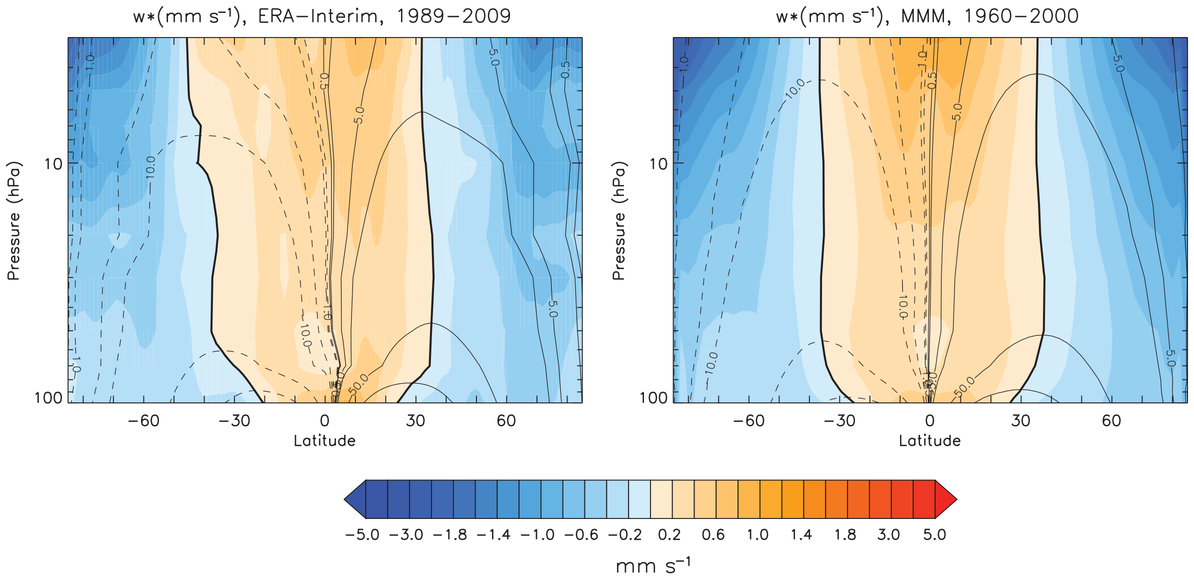


**Figure 1.** Annual mean residual vertical velocity, $\overline{w}^*$(mm s$^{-1}$), for ERA-Interim (1989–2009), and the CMIP5 models. Multi-model mean (MMM) values are shown, using historical simulations (1960–2000). The zero line is shown as a bold black contour. The stream function (kg m$^{-1}$s$^{-1}$) is shown in logarithmically spaced grey contours. Dashed contours represent negative values.

### 3.2. *Turn-around latitudes and tropical upwelling mass flux*

The tropical upwelling mass flux at height $z$ is

$$M(z) = 2\pi a\{\psi_{\max}(z) - \psi_{\min}(z)\}, \tag{4}$$

where $\psi_{\max}$ and $\psi_{\min}$ are the maximum/minimum values of $\psi$, which occur at the northern/southern turn-around latitudes (Rosenlof, 1995). Figure 2 shows climatological values for, and trends in, the turn-around latitudes and the tropical upwelling mass flux as a function of height. Seviour *et al.* (2012) point out that, in ERA-Interim, the width of the upwelling region at 70 hPa is 53.3% of the global surface area. The corresponding value for the multi-model mean is 56.4%. Thus on average the extratropical downwelling velocities are greater than the tropical upwelling velocities. Compared to ERA-Interim, the models are too hemispherically symmetric, missing the property that the southern turn-around latitude in the lower (upper) stratosphere is further equatorward (poleward) than the northern turn-around latitude.

Over the twenty-first century, the upwelling region becomes narrower in the lower stratosphere (below $\sim$ 20 hPa), and wider in the middle to upper stratosphere (from 20 to 3 hPa); Figure 2 shows turn-around latitude trends. This suggests possibly different mechanisms are responsible for the changes in these two altitude bands, as discussed further below. Consistent with Butchart *et al.* (2010), the upwelling mass flux is found to increase with climate change at all altitudes throughout the stratosphere. The percentage change in the upwelling mass flux (not shown) is 3.5% per decade at 70 hPa for the RCP 8.5 scenario analysed here, which as expected is larger than the 1.8% per decade obtained by Butchart *et al.* (2010) for the IPCC Special Report on Emissions Scenarios A1B scenario (due to the faster increase in greenhouse gas concentrations in RCP 8.5).

### 3.3. *Changes in planetary wave propagation*

Figure 3 shows the trend in $\overline{w}^*$ for the period 2006–2099. As mentioned in the last section, the increase in tropical upwelling occurs throughout the entire tropical stratosphere. In the lower stratosphere where the upwelling region becomes narrower, the largest increase in $\overline{w}^*$ is near the centre of the upwelling region, with values of more than 5% per decade. However, at higher levels where the upwelling region widens, $\overline{w}^*$ increases most towards the edges of the upwelling region.

In this section, the mechanisms leading to the changes in the position of the turn-around latitudes are considered. In steady-state conditions, the residual stream function, $\psi$, at a given log-pressure height, $z$, and latitude, $\phi$, is driven by the force from wave breaking at latitude $\phi$, and above log-pressure height $z$ (Eq. 2.5 in Haynes *et al.*, 1991). The Charney–Drazin criterion (Andrews *et al.*, 1987, p. 178) states that stationary waves (waves with zero phase speed) can only propagate in westerly zonal flow ($\overline{u} > 0$), thus $\overline{u} = 0$ is the 'critical line' for such waves, separating regions of wave propagation from regions of wave evanescence. Near the critical line, nonlinear effects will dominate (Andrews *et al.*, 1987, pp. 253–258) and stationary wave breaking will likely occur in the regions of weak zonal wind just poleward of the critical line. Therefore the turn-around latitudes (situated at the latitudes where $\psi$ is a maximum/minimum) are located poleward of the critical lines, as shown in Figure 3.

Figure 3 shows that, on average, the $\overline{u} = 0$ critical line in the CMIP5 models moves equatorward at all heights (from 100 to 3 hPa) by $\sim 4^\circ$ due to climate change. The width of the associated Rossby wave nonlinear critical layer, $\delta_{NL} = \left(a\widetilde{v}/k\overline{u}_\phi\right)^{1/2}$ ('Critical layers' in Warren and Hahn, 2003), where $\widetilde{v}$ is the amplitude of wave latitudinal velocity at the critical line and $k$ is zonal wavenumber, is found here to increase, throughout the twenty-first century, by at most $2^\circ$ (not shown). The equatorward movement of the critical line for stationary waves is therefore expected to dominate the changes in the location of wave breaking. However, as noted in the previous section, the turn-around latitudes only move equatorward below 20 hPa, and they move poleward from 20 to 3 hPa.

Figure 4 shows that the equatorward shift in the $\overline{u} = 0$ critical line position at all altitudes is due to $\overline{u}$ increasing almost everywhere in the tropical stratosphere under climate change (with the exception of two localised regions where the decrease in $\overline{u}$ is likely associated with the Quasi-Biennial Oscillation (QBO); note that the increase in the tropical stratosphere is not statistically significant). This result is in agreement with Shepherd and McLandress (2011) (for CMAM). In particular, in the lower stratosphere (below $\sim$ 20 hPa; the shallow branch of the Brewer–Dobson circulation), the subtropical jets get stronger due to climate change, and the centre of the jets shifts upwards and equatorwards (Figure 4; also Garcia and Randel, 2008; Li *et al.*, 2010). The consequent equatorward movement of the critical line in the lower stratosphere allows synoptic- and planetary-scale stationary waves to propagate further into the Tropics and higher into the stratosphere (Calvo and Garcia, 2009; Shepherd and

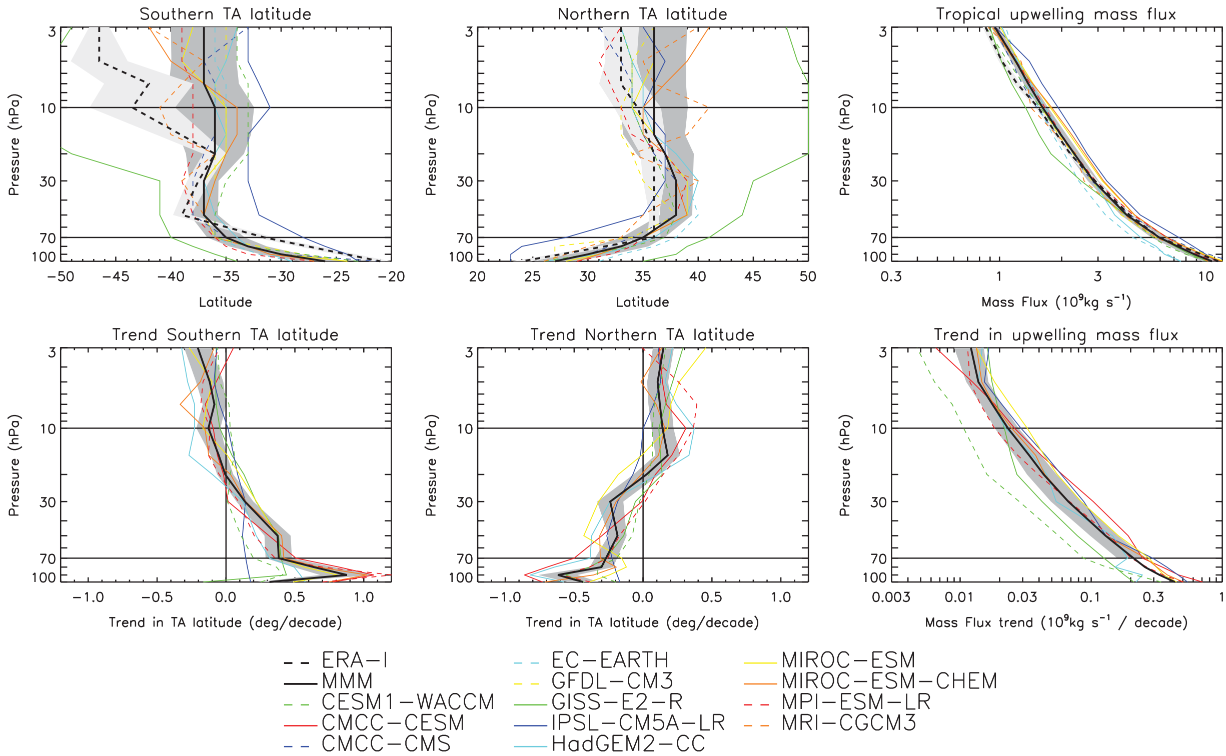


**Figure 2.** Upper panels: Turn-around latitudes calculated from annual mean $\overline{w}^*$(mm s$^{-1}$) climatologies for ERA-Interim (1989–2009) and models (1960–2000). Dashed black lines show the turn-around latitudes for ERA-Interim, with light grey shading showing the interannual standard deviation, scaled to represent a 95% confidence interval. Solid black lines show turn-around latitudes for the multi-model mean $\overline{w}^*$, with dark grey shading showing inter-model standard error, scaled to represent a 95% confidence interval. Individual model turn-around latitudes are shown by thin coloured lines, as specified in the key. Tropical upwelling is calculated for each year, as the mass upwelling between turn-around latitudes, and then averaged (1960–2000 for the models, and 1989–2009 for ERA-Interim). Lower panels: Trend in the turn-around latitudes and upwelling mass flux for the models, using a linear fit to years 2006–2099 from the RCP 8.5 scenario simulations, with dark grey shading showing inter-model standard error as above. Thin horizontal lines are shown at 70 and 10 hPa to aid comparison to previous studies. Note that, as discussed in detail by Hardiman *et al.* (2007), the turn-around latitudes of the mean $\overline{w}^*$, and their trends, are not equal to the mean of the individual model turn-around latitudes and their trends.

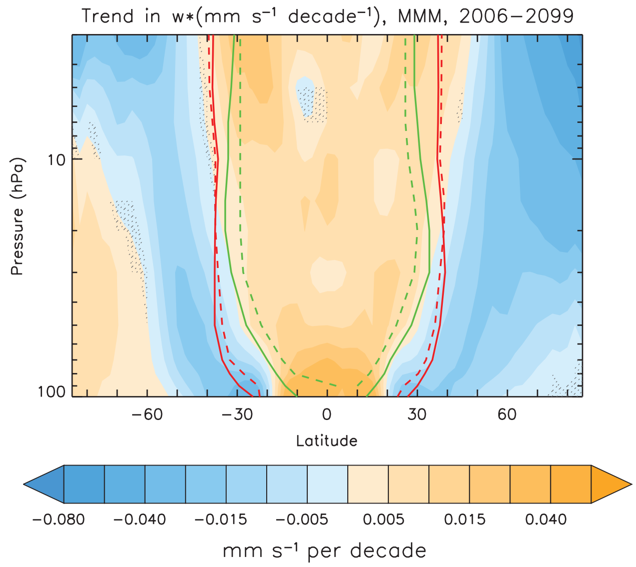


**Figure 3.** Contours show trend in $\overline{w}^*$(mm s$^{-1}$decade$^{-1}$) using a linear fit to years 2006–2099 from the RCP 8.5 scenario simulations. Red lines show the turn-around latitudes, with solid lines showing the mean position for the period 2006–2025, and dashed lines showing the mean position for the period 2080–2099. Green lines show the stationary wave critical lines, $\overline{u} = 0$, with solid lines showing positions where multi-annual mean $\overline{u}$(2006–2025) is zero, and dashed lines showing positions where multi-annual mean $\overline{u}$(2080–2099) is zero. Stippling shows regions where the trend is NOT significant at the 95% level.

McLandress, 2011), with a subsequent equatorward movement of the turn-around latitudes.

On the other hand, in the upper stratosphere (above $\sim$ 20 hPa; the deep branch of the Brewer–Dobson circulation), the equatorward movement of the critical line does not appear to be the main factor in driving the change in the turn-around latitudes. Instead, Figure 4 shows that the maximum increase in $\overline{u}$ in the upper stratosphere occurs in the region 50°–60°N, a behaviour dominated by the winter hemisphere (not shown). Estimating the wave refractive index (which assumes linear waves propagating on a slowly varying background flow; Matsuno, 1970) from the monthly mean dynamical fields, it is found that the equatorward refraction of the upward propagating planetary waves in the winter hemisphere is weakened due to climate change, most likely due to the increasing $\overline{u}$ in midlatitudes. This will contribute to the poleward movement of the turn-around latitudes. Furthermore, the explicitly calculated stationary (monthly mean) component of the Eliassen–Palm flux (Andrews *et al.*, 1987) also indicates a reduced equatorward refraction in the planetary wave flux in the upper stratosphere (not shown). Whilst this stationary component may not be representative of changes in the full Eliassen–Palm flux, the fact that this diagnostic shows a consistent change to that in the wave-refractive index adds weight to our conclusions. In addition, gravity wave drag might also play an important role in the upwelling trends in the upper stratosphere, as shown by Garcia and Randel (2008) for the Whole-Atmosphere Community Climate Model (WACCM). Unfortunately, the contribution of gravity wave drag cannot be assessed in this study, as diagnostics of gravity wave drag are not available.

In summary, we have shown that linear wave theory, as applied to stationary waves, can explain the simulated changes in the turn-around latitudes due to climate change, although the role of transient resolved waves and gravity waves remains to be investigated.

## 4. Seasonal cycle

Figure 5 shows the multi-model mean climatological $\overline{w}^*$ (1960–2000) at 70 hPa as a function of latitude and month,

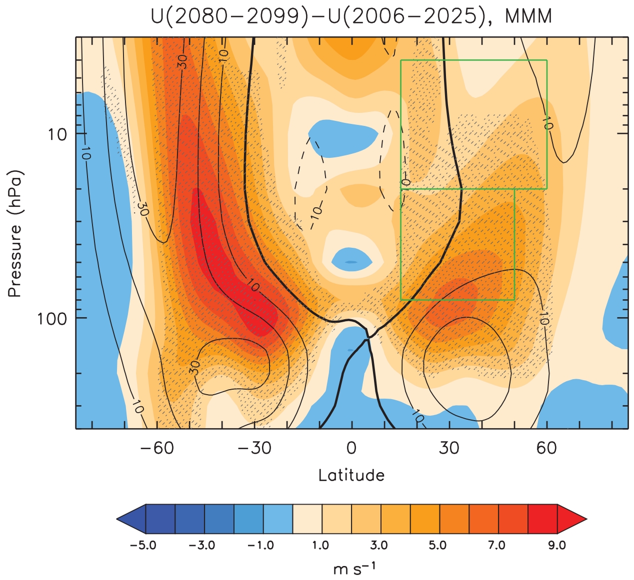


**Figure 4.** Black contours show $\overline{u}$ climatology (2006–2025) and the shading shows the difference $\overline{u}$(2080–2099) minus $\overline{u}$(2006–2025), in the RCP 8.5 scenario simulations. Stippling shows regions where the change in $\overline{u}$ is significant at the 95% level. The green boxes indicate regions referred to as 'lower stratosphere' and 'upper stratosphere' in the text.

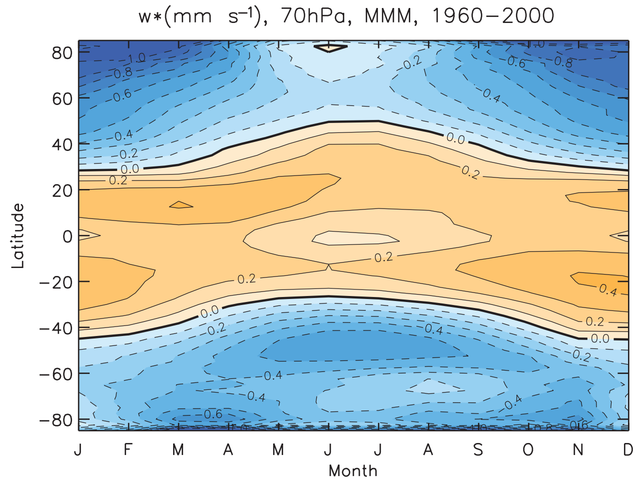


**Figure 5.** The multi-model mean (MMM) seasonal cycle of the latitudinal distribution of $\overline{w}^*$(mm s$^{-1}$) at 70 hPa, averaged 1960–2000 (historical simulations).

showing the seasonal cycle of the tropical upwelling region (similar to the behaviour in ERA-Interim shown in Figure 4 of Seviour *et al.*, 2012). The upwelling region is always displaced towards the summer hemisphere, and the extratropical downwelling is strongest in the winter hemisphere. As the width of the upwelling region changes due to climate change, the amplitude of the seasonal cycle in the centre of the upwelling region, defined as (DJF centre − JJA centre)/2, is found to decrease by around 2°, or by around 10% of its current value, throughout the stratosphere by the end of the twenty-first century (not shown).

As the amount of tropical upwelling increases, due to climate change, this must be balanced in the models by an increase in the extratropical downwelling. Figure 6 shows the climatology (2006–2025) and climate change response [(2080–2099) minus (2006–2025)] in $\overline{w}^*$ at four different altitudes. Left hand panels show how the seasonal cycle in the upwelling region varies with height. The turn-around latitudes in the summer hemispheres extend to the poles in the mid to upper stratosphere.

As was shown in Figure 3, the maximum increase due to climate change in $\overline{w}^*$ in the Tropics is displaced further from the Equator with increasing altitude. Consistent with this, the right hand panels of Figure 6 show that, in the Northern Hemisphere, increased downwelling occurs predominantly in the midlatitudes at altitudes for which there is an equatorward trend in the turn-around latitudes (below ∼ 20 hPa) and predominantly at polar latitudes at altitudes for which there is a poleward trend in the turn-around latitudes (above ∼ 20 hPa). In the Southern Hemisphere, however, there is an additional (superimposed) response of *decreased* downwelling at polar latitudes for the months July to December, likely due to ozone recovery. It is important to note that, although the changes in Figure 6 in the lowermost stratosphere are very robust across models in the Tropics and midlatitudes (90% significance shown by stippling at 70 and 30 hPa), the agreement across models is not so great in the upper stratosphere (70% significance shown by stippling at 10 and 3 hPa).

Figure 7 quantifies this change in the downwelling in the seasonal means. In December–February the increased tropical upwelling due to climate change is balanced predominantly by an increased downwelling in the Northern (winter) Hemisphere. Most of the increased downwelling occurs in midlatitudes below 10 hPa (with maximum 3.2% occurring at 50°N and 20 hPa), and at polar latitudes above 10 hPa (with peak values at 3 hPa occurring between 60° and 70°N). However, in June–August, due to the much stronger Southern Hemisphere winter stratospheric polar night jet, most of the increased downwelling occurs in the midlatitudes at all altitudes (with peak values in a large region from 40° to 50°S and 40 to 10 hPa). In both seasons there is reduced downwelling in the polar latitudes in the Southern Hemisphere lower stratosphere which, as suggested above, is likely due to ozone recovery. This reduced downwelling is strongest in September–November (not shown). Note also that there is significantly increased downwelling in both hemispheres within the region of the shallow branch of the Brewer–Dobson circulation (below ∼ 30 hPa), but significantly increased downwelling only in the winter hemisphere within the region of the deep branch (above ∼ 30 hPa). The winter hemispheres dominate the annual mean response (not shown).

## 5. Conclusions

In this article, the spatial structure of the Brewer–Dobson circulation has been analysed in the CMIP5 models. This is the first multi-model study of the Brewer–Dobson circulation using coupled ocean–atmosphere models with a well-resolved stratosphere.

Under climate change, the tropical upwelling mass flux, commonly used to measure the strength of the Brewer–Dobson circulation, increases at every altitude throughout the stratosphere. This is of relevance both to the transport of chemical species throughout the stratosphere and to tropical phenomena, such as the QBO (Baldwin *et al.*, 2001) and the stratospheric water vapour 'tape-recorder' (Mote *et al.*, 1996). Indeed, for the models studied in this article, around 20% of the total mass upwelling occurs between 5°S and 5°N, a region commonly used for diagnosing the QBO, and around 60% of the total mass upwelling occurs between 20°S and 20°N, the tape-recorder region (Gettelman *et al.*, 2010).

Not only does the magnitude of the tropical upwelling increase, but the *width* of the tropical upwelling region changes, narrowing below around 20 hPa, and increasing above 20 hPa (up to a height of around 3 hPa), suggesting that different physical mechanisms are responsible for the changes above and below 20 hPa. Below 20 hPa, the upward displacement and strengthening of the subtropical jets, and the subsequent equatorward shift in the critical lines, leads to synoptic- and planetary-scale waves propagating further into the Tropics (Calvo and Garcia, 2009; Shepherd and McLandress, 2011). However, above 20 hPa the equatorward shift of the critical lines does not play an important role. The increase in the winter hemisphere extratropical zonal mean wind strength leads to a reduced equatorward refraction of the planetary waves, as implied by

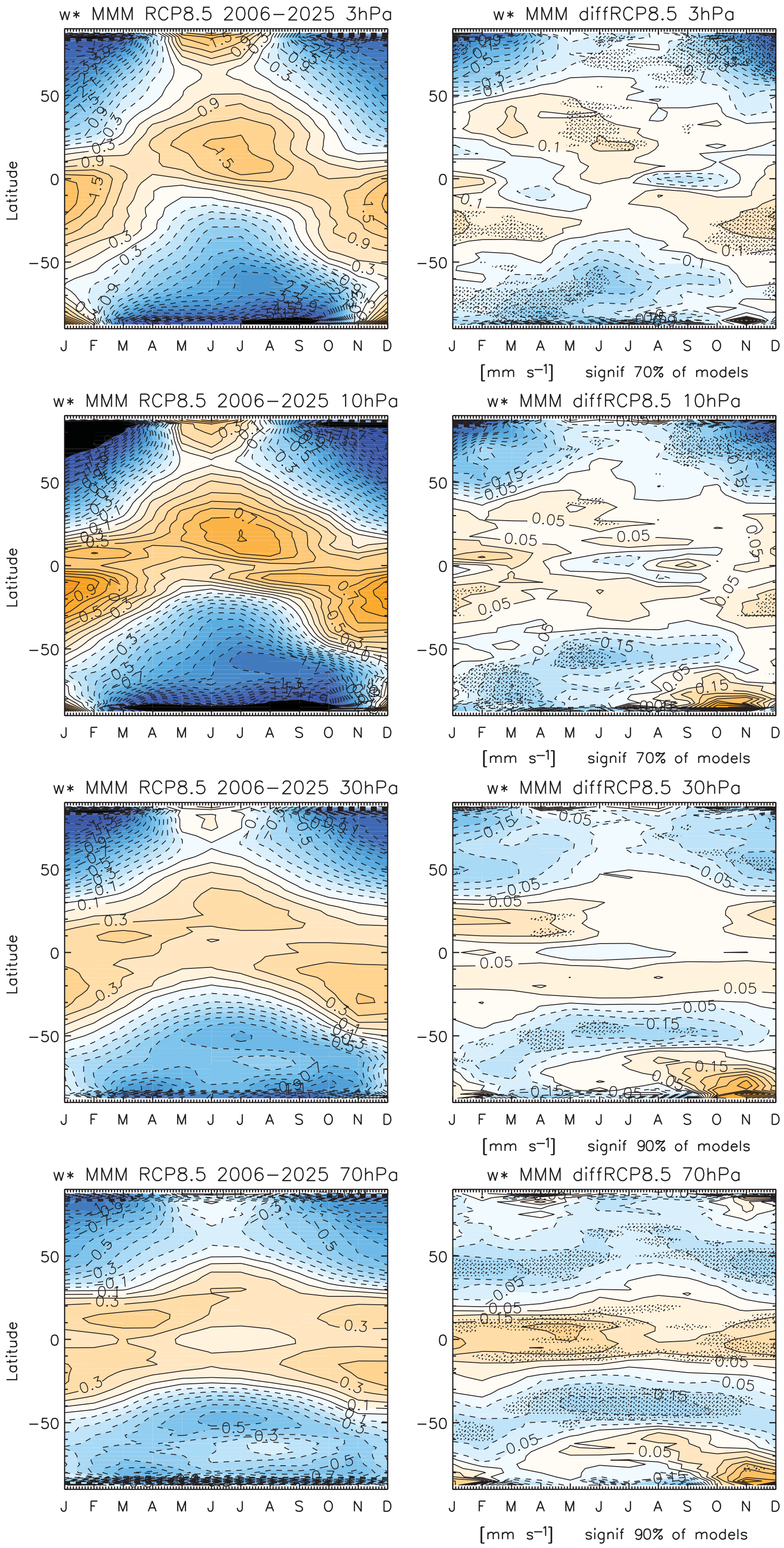


**Figure 6.** Left panels show the seasonal cycle of the latitudinal distribution of $\overline{w}^{*}$ (mm s$^{-1}$) averaged 2006–2025, and right panels show the climate change response [(2080–2099) minus (2006–2025)] in the RCP 8.5 scenario simulations. Stippling in the right panels shows regions where at least 70% (at 3 and 10 hPa) or 90% (at 30 and 70 hPa) of the models show a significant response at the 95% level. Contour intervals are 0.1 mm s$^{-1}$ (left panels) and 0.05 mm s$^{-1}$ (right panels) for 70, 30, and 10 hPa, and are 0.3 mm s$^{-1}$ (left panel) and 0.1 mm s$^{-1}$ (right panel) for 3 hPa.

the wave-refractive index (assuming linear waves propagating on a slowly varying background flow). This likely contributes to the poleward shift in the turn-around latitudes at these heights. To add weight to this conclusion, the explicitly calculated steady state (monthly mean) component of the Eliassen–Palm flux is found also to show a poleward refraction due to climate change at these heights, though this may not represent the behaviour of the full Eliassen–Palm flux. The effects of gravity waves were not considered in the analysis of this study, but are also believed to significantly contribute to the Brewer–Dobson circulation trends in the upper stratosphere (Garcia and Randel, 2008).

The increase in tropical upwelling due to climate change is balanced by an increase in the extratropical downwelling. In the Northern Hemisphere, this increased downwelling is

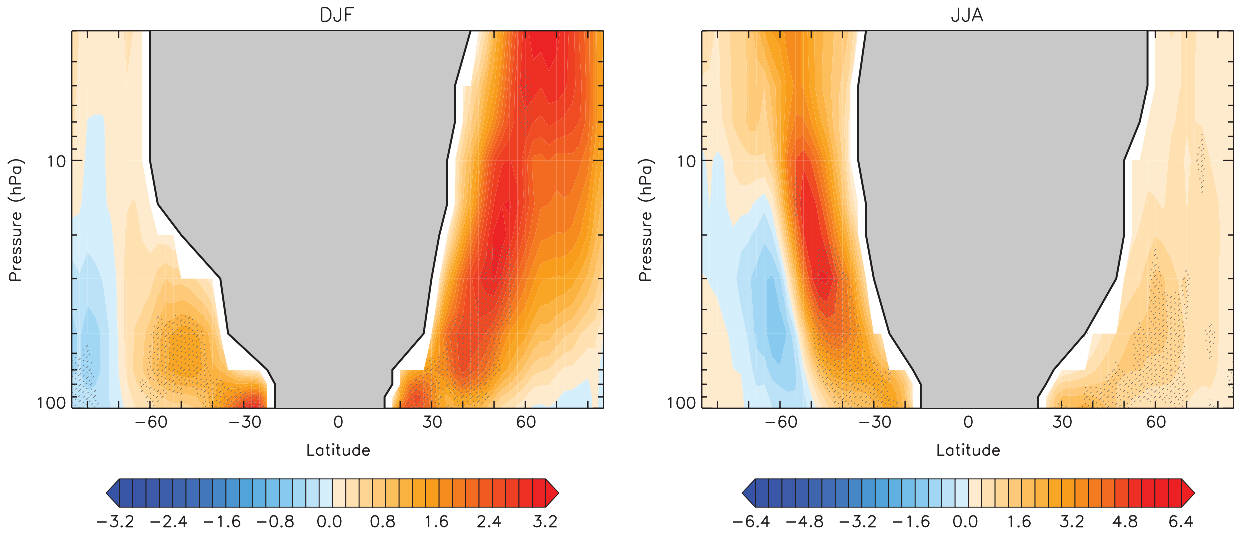


**Figure 7.** Ratio at each altitude of the change in extratropical downwelling mass flux to the change in total tropical upwelling mass flux [(2080–2099) minus (2006–2025)], for all latitudes outside the upwelling region (multi-model mean; expressed at each degree of latitude as a percentage of the total downwelling). Regions of reduced extratropical downwelling show as negative ratios. Black lines show the turn-around latitudes, with the upwelling region shaded grey. Stippling shows regions where at least 90% of the models show a significant climate change response in $\overline{w}^*$ at the 95% level. As in Figure 6, significance decreases with altitude.

seen mainly in midlatitudes at altitudes where the turn-around latitudes shift equatorward, and mainly in the polar latitudes in the upper stratosphere where there is a poleward trend in the turn-around latitudes. In the Southern Hemisphere, the increased downwelling is seen at midlatitudes throughout the stratosphere, and there is reduced downwelling in the polar latitudes. This suggests an increased wave-driven transport of ozone to the northern high latitudes, but not necessarily to the southern high latitudes (Tegtmeier *et al.*, 2008). It further suggests a hemispheric asymmetry in any influence of the changing Brewer–Dobson circulation on tropospheric weather patterns through, for example, the position of the tropospheric storm tracks (Scaife *et al.*, 2011), though it must be noted that the storm tracks also have hemispheric asymmetry due to different land masses and regardless of the Brewer–Dobson circulation.

For the reasons highlighted above, it is suggested that future studies on the Brewer–Dobson circulation focus not only on the increasing tropical troposphere-to-stratosphere mass flux, but also on the changing vertical and latitudinal structure of the circulation throughout the twenty-first century.

## Acknowledgements

The authors are very grateful to Thomas Birner and Charles McLandress for their comments on a previous version of this manuscript. The work of SCH and NB was supported by the Joint DECC/Defra Met Office Hadley Centre Climate Programme (GA01101) and also by the European Commission's Seventh Framework Programme, under Grant Agreement number 226520, COMBINE project. NC is partly supported by the Spanish Ministry of Science, through the project Supercomputing and e-Science, Consolider CSD 2007-00050. Model data were supplied by Chiara Cagnazzo, Bo Christiansen, François Lott, Elisa Manzini, Daniel Marsh, Drew Shindell, Evgeny Volodin, Shingo Watanabe, John Wilson and Seiji Yukimoto. ERA-Interim data used in this study were provided by the European Centre for Medium-range Weather Forecasting.

## References

Andrews DG, Holton JR, Leovy CB. 1987. *Middle Atmosphere Dynamics*. Academic Press: San Diego, CA.

Baldwin MP, Gray LJ, Dunkerton TJ, Hamilton K, Haynes PH, Randel WJ, Holton JR, Alexander MJ, Hirota I, Horinouchi T, Jones DBA, Kinnersley JS, Marquardt C, Sato K. 2001. The quasi-biennial oscillation. *Rev. Geophys.* **39**: 179–230, doi: 10.1029/1999RG000073.

Birner T, Boenisch H. 2011. Residual circulation trajectories and transit times into the extratropical lowermost stratosphere. *Atmos. Chem. Phys.* **11**: 817–827, doi: 10.5194/acp-11-817-2011.

Boenisch H, Engel A, Birner T, Hoor P, Tarasick DW, Ray EA. 2011. On the structural changes in the Brewer–Dobson circulation after 2000. *Atmos. Chem. Phys.* **11**: 3937–3948, doi: 10.5194/acp-11-3937-2011.

Butchart N, Scaife AA. 2001. Removal of chlorofluorocarbons through increased mass exchange between the stratosphere and troposphere in a changing climate. *Nature* **410**: 799–801.

Butchart N, Scaife AA, Bourqui M, de Grandpré J, Hare SHE, Kettleborough J, Langematz U, Manzini E, Sassi F, Shibata K, Shindell D, Sigmond M. 2006. Simulations of anthropogenic change in the strength of the Brewer-Dobson circulation. *Clim. Dyn.* **27**: 727–741.

Butchart N, Cionni I, Eyring V, Shepherd TG, Waugh DW, Akiyoshi H, Austin J, Brühl C, Chipperfield MP, Cordero E, Dameris M, Deckert R, Dhomse S, Frith SM, Garcia RR, Gettelman A, Giorgetta MA, Kinnison DE, Li F, Mancini E, McLandress C, Pawson S, Pitari G, Plummer DA, Rozanov E, Sassi F, Scinocca JF, Shibata K, Steil B, Tian W. 2010. Chemistry-climate model simulations of 21st century stratospheric climate and circulation changes. *J. Clim.* **23**: 5349–5374.

Caesar J, Palin E, Liddicoat S, Lowe J, Burke E, Pardaens A, Sanderson M, Kahana R. 2013. Response of the HadGEM2 Earth System Model to future greenhouse gas emissions pathways to the year 2300. *J. Clim.* **26**: 3275–3284, doi: 10.1175/JCLI-D-12-00577.1.

Calvo N, Garcia RR. 2009. Wave forcing of the tropical upwelling in the lower stratosphere under increasing concentrations of greenhouse gases. *J. Atmos. Sci.* **66**: 3184–3196, doi: 10.1175/2009JAS3085.1.

Charlton-Perez AJ, Baldwin MP, Birner T, Black RX, Butler AH, Calvo N, Davis NA, Gerber EP, Gillett N, Hardiman SC, Kim J, Krüger K, Lee Y-Y, Manzini E, McDaniel BA, Polvani L, Reichler T, Shaw TA, Sigmond M, Son S-W, Toohey M, Wilcox L, Yoden S, Christiansen B. 2013. On the lack of stratospheric dynamical variability in low-top versions of the CMIP5 models. *J. Geophys. Res.–Atmos.* **118**: 2494–2505, doi: 10.1002/jgrd.50125.

Dee DP, Uppala SM, Simmons AJ, Berrisford P, Poli P, Kobayashi S, Andrae U, Balmaseda MA, Balsamo G, Bauer P, Bechtold P, Beljaars ACM, van de Berg L, Bidlot J, Bormann N, Delsol C, Dragani R, Fuentes M, Geer AJ, Haimberger L, Healy SB, Hersbach H, Hólm EV, Isaksen L, Kållberg P, Köhler M, Matricardi M, McNally AP, Monge-Sanz BM, Morcrette J-J. 2011. The ERA-Interim reanalysis: Configuration and performance of the data assimilation system. *Q. J. R. Meteorol. Soc.* **137**: 553–597.

Garcia RR, Randel WJ. 2008. Acceleration of the Brewer-Dobson circulation due to increases in greenhouse gases. *J. Atmos. Sci.* **65**: 2731–2739, doi: 10.1175/2008JAS2712.1.

Gettelman A, Hegglin MI, Son S-W, Kim J, Fujiwara M, Birner T, Kremser S, Rex M, Añel JA, Akiyoshi H, Austin J, Bekki S, Braesike P, Brühl C, Butchart N, Chipperfield M, Dameris M, Dhomse S, Garny H, Hardiman SC, Jöckel P, Kinnison DE, Lamarque JF, Mancini E, Marchand M, Michou M, Morgenstern O, Pawson S, Pitari G, Plummer D, Pyle JA, Rozanov E, Scinocca J, Shepherd TG, Shibata K, Smale D, Teyssèdre H, Tian W. 2010. Multimodel assessment of the upper troposphere and lower stratosphere: Tropics and global trends. *J. Geophys. Res.* **115**: D00M08, doi: 10.1029/2009JD013638.

Hardiman SC, Butchart N, Haynes PH, Hare SHE. 2007. A note on forced versus internal variability of the stratosphere. *Geophys. Res. Lett.* **34**: L12803, doi: 10.1029/2007GL029726.

Haynes PH, Marks CJ, McIntyre ME, Shepherd TG, Shine KP. 1991. On the 'downward control' of extratropical diabatic circulations by eddy-induced mean zonal forces. *J. Atmos. Sci.* **48**: 651–678.

Hazeleger W, Severijns C, Semmler T, Ştefănescu S, Yang S, Wang X, Wyser K, Dutra E, Baldasano JM, Bintanja R, Bougeault P, Caballero R, Ekman AML, Christensen JH, van den Hurk B, Jimenez P, Jones C, Kållberg P, Koenigk T, McGrath R, Miranda P, Noije TV, Palmer T, Parodi JA, Schmith T, Selten F, Storelvmo T, Sterl A, Tapamo H, Vancoppenolle M, Viterbo P, Willén U. 2010. EC-Earth: A seamless earth system prediction approach in action. *Bull. Am. Meteorol. Soc.* **91**: 1357–1363, doi: 10.1175/2010BAMS2877.1.

Jones CD, Hughes JK, Bellouin N, Hardiman SC, Jones GS, Knight J, Liddicoat S, O'Connor FM, Andres RJ, Bell C, Boo K-O, Bozzo A, Butchart N, Cadule P, Corbin KD, Doutriaux-Boucher M, Friedlingstein P, Gornall J, Gray L, Halloran PR, Hurtt G, Ingram WJ, Lamarque JF, Law RM, Meinshausen M, Osprey S, Palin EJ, Parsons Chini L, Raddatz T, Sanderson MG, Sellar AA, Schurer A, Valdes P, Wood N, Woodward S, Yoshioka M, and Zerroukat M. 2011. The HadGEM2-ES implementation of CMIP5 centennial simulations. *Geosci. Model Dev.* **4**: 543–570, doi: 10.5194/gmd-4-543-2011.

Li F, Stolarski RS, Pawson S, Newman PA, Waugh D. 2010. Narrowing of the upwelling branch of the Brewer–Dobson circulation and Hadley cell in chemistry–climate model simulations of the 21st century. *Geophys. Res. Lett.* **37**: L13702, doi: 10.1029/2010GL043718.

Lott F, Fairhead L, Hourdin F, Levan P. 2005. The stratospheric version of LMDz: Dynamical climatologies, arctic oscillation, and impact on the surface climate. *Clim. Dyn.* **25**: 851–868, doi: 10.1007/s00382-005-0064-x.

Marsh DR, Mills MJ, Kinnison DE, Lamarque J-F, Calvo N, Polvani LM. 2013. Climate change from 1850 to 2005 simulated in CESM1(WACCM). *J. Clim.* **26**: 7372–7391.

Matsuno T. 1970. Vertical propagation of stationary planetary waves in the winter Northern Hemisphere. *J. Atmos. Sci.* **27**: 871–883.

McLandress C, Shepherd TG. 2009. Simulated anthropogenic changes in the Brewer–Dobson circulation, including its extension to high latitudes. *J. Clim.* **22**: 1516–1540.

Moss RH, Edmonds JA, Hibbard KA, Manning MR, Rose SK, van Vuuren DP, Carter TR, Emori S, Kainuma M, Kram T, Meehl GA, Mitchell JFB, Nakicenovic N, Riahi K, Smith SJ, Stouffer RJ, Thomson AM, Weyant JP, Wilbanks TJ. 2010. The next generation of scenarios for climate change research and assessment. *Nature* **463**: 747–756, doi: 10.1038/nature08823.

Mote PW, Rosenlof KH, McIntyre ME, Carr ES, Gille JC, Holton JR, Kinnersley JS, Pumphrey HC, Russell JM III, Waters JW. 1996. An atmospheric tape recorder: The imprint of tropical tropopause temperatures on stratospheric water vapor. *J. Geophys. Res.* **101**: 3989–4006, doi: 10.1029/95JD03422.

Neu JL, Plumb RA. 1999. Age of air in a 'leaky pipe' model of stratospheric transport. *J. Geophys. Res.* **104**: 19243–19255.

Plumb RA. 2002. Stratospheric transport. *J. Meteorol. Soc. Jpn.* **80**: 793–809.

Riahi K, Gruebler A, Nakicenovic N. 2007. Scenarios of long-term socio-economic and environmental development under climate stabilization. *Technol. Forecasting Social Change* **74**: 887–935.

Rosenlof KH. 1995. Seasonal cycle of the residual mean meridional circulation in the stratosphere. *J. Geophys. Res.* **100**: 5173–5191, doi: 10.1029/94JD03122.

Scaife AA, Spangehl T, Fereday DR, Cubasch U, Langematz U, Akiyoshi H, Bekki S, Braesicke P, Butchart N, Chipperfield MP, Gettelman A, Hardiman SC, Michou M, Rozanov E, Shepherd TG. 2011. Climate change projections and stratosphere-troposphere interaction. *Clim. Dyn.* **38**: 2089–2097, doi: 10.1007/s00382-011-1080-7.

Seviour WJM, Butchart N, Hardiman SC. 2012. The Brewer–Dobson circulation inferred from ERA-Interim. *Q. J. R. Meteorol. Soc.* **138**: 878–888, doi: 10.1002/qj.966.

Shepherd TG, McLandress C. 2011. A robust mechanism for strengthening of the Brewer–Dobson circulation in response to climate change: Critical-layer control of subtropical wave breaking. *J. Atmos. Sci.* **68**: 784–797.

Tegtmeier S, Rex M, Wohltmann I, Krüger K. 2008. Relative importance of dynamical and chemical contributions to Arctic wintertime ozone. *Geophys. Res. Lett.* **35**: L17801, doi: 10.1029/2008GL034250.

Warren SG, Hahn J. 2003. Cloud climatology. In *Encyclopedia of Atmospheric Sciences*, Holton JR, Curry JA, Pyle JA. (eds.) 476–483: Academic Press: San Diego, CA.